An Optimized Control Method for Firing Angle of Hybrid Line Commutated Converter During AC Faults

Jianchao Ma, Xiaoping Zhou, *Member*, *IEEE*, Lingfeng Deng, Lerong Hong, *Member*, *IEEE*, Hanting Peng, Yizhen Hu, Lei Zhang, Fenfen Zhu, Haitao Xia, and Honglin Ouyang

***Abstract*—The introduction of fully controlled devices to build hybrid line commutated converter (H-LCC) has become a new idea to solve the commutation failure. However, existing H-LCC has not considered the implementation of a targeted firing angle control strategy during AC faults, with the objective of enhancing their power transmission and fault response performance. For this reason, this paper proposes an optimized control method for firing angle of H-LCC, designated as flexible virtual firing (FVF). This method first analyzes the influence of alterations in firing angle on reactive power, commutation process and associated action paths. By combining prediction and dynamic search, it optimizes the natural commutation process through the utilization of dynamic boundary and minimum commutation area difference. This can mitigate the impact of AC faults on H-LCC and DC system, thereby improving power transmission and defense to commutation failure, which is beneficial for improving the stability of AC/DC power grids. Finally, the simulation results in PSCAD/EMTDC verify the effectiveness of the proposed method.**

***Index Terms*—Commutation failure, fully controlled device, firing angle optimization, optimal control, hybrid line commutated converter.**

I. Introduction

LINE commutated converter based high-voltage direct current (LCC-HVDC) has been widely utilized in the field of large-capacity and long-distance power transmission due to the numerous advantages, including low loss, low cost, high transmission capacity and mature technology [1]. LCC-HVDC uses semi-controlled device that requires a certain degree of commutation support from the AC system. Therefore, it is inevitable that certain problems emerge, especially the commutation failure (CF) cannot be avoided all the time [2]. Once the CF occurs, the DC current increases rapidly, and the DC voltage and transmission power decrease rapidly. In severe cases, it causes DC system lockout [3]. As the number of DC points integrated into existing load centers continues to increase, the risk probability of CF and cascading failure have increased sharply in the multi-feed DC transmission system. This has become a significant problem that endangers the secure and stable operation of AC/DC power grids [4].

In order to solve the aforementioned problems, related researches have primarily concentrated on two aspects for modifying LCC-HVDC. One is to improve its control and protection system. For example, commutation failure prevention (CFPREV) control is improved from different perspectives to enhance the ability to defense CF as much as possible [5], [6]. However, such method has limited effect in the presence of severe fault conditions. Furthermore, it also increases the reactive power consumption of the converter and results in further reduction in AC voltage, which may have a detrimental impact on the commutation process [7]. In comparison, the topology modification of LCC has been investigated due to its obvious effects. Reference [8] proposes capacitor commutated converter (CCC) based HVDC, which increases the steady-state commutation angle by inserting a fixed series capacitor between the secondary winding part of the transformer and the bridge arm of the converter. However, the addition of capacitors may lead to charging overvoltage, causing the inverter to lose its self-recovery ability. Controlled series capacitor converter (CSCC) changes the position of the series capacitor between the system and the converter transformer [9], but the harmonic characteristics of this topology are complex and there is a risk of resonance. Similarly, there are evolutional line commutated converter (ELCC) [10], evolved capacitor commutated converter (ECCC) [11], serially connecting resistors on capacitor branch [12], etc.

Manuscript received: February 7, 2024; revised: May 4, 2024; accepted: August 5, 2024. Date of CrossCheck: August 5, 2024. Date of online publication: August 26, 2024.

This work was supported in part by the National Key Research and Development Program of China (No. 2021YFB2400900), the Integration Projects of National Natural Science Foundation of China-State Grid Joint Fund for Smart Grid (No. U2166602), the National Natural Science Foundation of China (No. 52207200), and the Science and Technology Innovation Program of Hunan Province (No. 2024RC3113).

J. Ma, X. Zhou (corresponding author), L. Deng, L. Hong, H. Peng, Y. Hu, L. Zhang, H. Ouyang are with the College of Electrical and Information Engineering, Hunan University, Changsha 410082, China (e-mail: jianchaoma2020@163.com; zxp2011@hnu. edu. cn; 18361228606@163. com; hlr0908@163. com; penghanting_hnu@163.com; huyizhen168@126.com; zl1192157465@163.com; oyhl1405.ouyang@vip.sina.com).

F. Zhu is with the State Grid Wuhu Electric Power Supply Company, Wuhu 241000, China (e-mail: zhuff2000@163.com).

H. Xia is with the China Railway Construction Heavy Industry Corporation Limited, Changsha 410082, China (e-mail: xht0903@163.com).

DOI: 10.35833/MPCE.2024.000148

Although some of the above methods involve fully controlled devices, their ultimate purpose is to use capacitors or resistor-capacitor to provide auxiliary commutation voltage and suppress fault current, thereby achieving auxiliary commutation. However, the utilization of fully controlled devices to directly turn off current has more significant advantages in solving CF. Therefore, [13] adopts double-terminal hybrid DC transmission, where the inverter side is modified to modular multilevel converter (MMC) structure based on the insulated gate bipolar transistor (IGBT). However, the technology route of MMC for UHVDC is characterized by high equipment costs, low power density, and high operating loss. Furthermore, it is also difficult to increase the capacity of IGBT, and the power matching contradiction is prominent. Besides, the coordination of control and protection between converters with different characteristics is complicated. Therefore, the technology route of MMC for ultra high-voltage direct current (UHVDC) is not obvious in large-capacity and long-distance power transmission [14].

The construction of hybrid line commutated converter (H-LCC) benefits from the recent rapid development of power electronic devices. H-LCC has been developed by modifying the LCC with fully controllable devices. This converter has the ability to self-shutdown and has lower operating losses and costs than the MMC. Reference [15] proposes an H-LCC structure in which thyristors and fully controllable devices are connected in series. IGBTs with reverse-parallel diodes are used in the fully controllable device. However, the difference in characteristics between IGBTs and thyristors causes new problems when they are turned off. Therefore, [16] proposes an H-LCC structure based on the double-branch parallel connection of thyristors and IGBTs, named controllable line-commutated converter (CLCC). In this topology, the bridge arm is divided into two sub-branches. The thyristor and IGBT are connected in series to form the main branch to carry large currents. The other auxiliary branch composed of IGBT is connected in parallel with the main branch in order to break current transferred from the main branch. Different from IGBT, integrated gate commutated thyristor (IGCT) is a fully controllable device developed on the basis of thyristor, both of which are current mode devices. The characteristics of the devices are similar to thyristor, with which series voltage balance is easier to achieve and the conduction voltage is also much lower than that of other fully controllable devices [17]. Following the release of the 2500 V/3000 A reverse blocking IGCT (RB-IGCT) by ABB in 2019 [18], the forward and reverse blocking voltage capabilities of RB-IGCT, as well as its high current conduction and maximum turn-off current capability in similar device, are ideal for constructing H-LCC [19]. Therefore, [20] proposes a novel H-LCC topology wherein RB-IGCTs are connected in series to replace the thyristors in the bridge arms according to a certain proportion. On this basis, [21] deeply analyzes the key factors such as device characteristics and shutdown principle, and provides a detailed application of this topology in the transformation of LCC-HVDC. The experiment results have demonstrated that this topology is highly economical and efficient, with considerable potential for further development [22].

The above research works on H-LCC primarily concentrate on the turn-off characteristics, aiming to use fully controllable devices to turn off the current when CF is about to occur. Although CF can be greatly alleviated or suppressed by this way, traditional LCC-HVDC control is still used, particularly the firing angle control. During AC faults, the constant extinction angle control might result in H-LCC being unable to fully leverage the advantages of controllable commutation, further enhancing the ability of fault response performance and suppressing CF. Therefore, this paper proposes a flexible virtual firing (FVF) control based on optimizing the firing angle of H-LCC. This optimized control method can better reduce the reactive power consumption of H-LCC, achieve DC transmission power during AC faults, and ensure the performance recovery and stability of the AC system. With the same ratio of fully controllable device, the CF suppression ability of H-LCC can also be improved.

II. Influence of Firing Angle on H-LCC Commutation Process

A. Basic Principles of H-LCC Commutation Process

As H-LCC is modified based on LCC, the commutation process from VT6 to VT2 on the inverter side of LCC-HVDC is first analyzed as an example, as shown in Fig. 1. The equivalent circuit of the inverter is also presented.

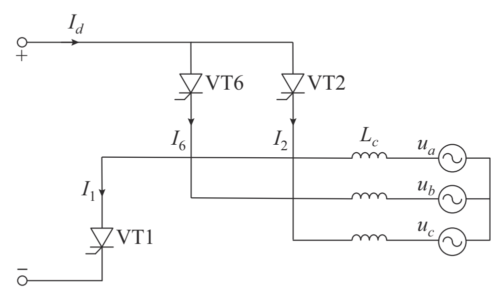

Fig. 1. Commutation process on inverter side.

The KVL equation of the two commutation circuits is:

$$u_b - u_c = L_c\left(\frac{\mathrm{d}i_2}{\mathrm{d}t} - \frac{\mathrm{d}i_6}{\mathrm{d}t}\right) \tag{1}$$

where u_b and u_c are the phase-B and phase-C voltages on the AC side, respectively; L_c is the equivalent commutation inductance; and i_2 and i_6 are the currents passed on VT2 and VT6, respectively.

The commutation voltage provided by the AC system on inverter side is $u_{bc} = \sqrt{2}\,E\sin(\omega t)$, where E is the root mean square (RMS) of AC line-to-line voltage and ω is the angular frequency. The DC current during commutation is $I_d = i_2 + i_6$. These two equations are substituted into (1) and integrated on both sides of the equation:

$$\sqrt{2}\,E\int_{\frac{\alpha}{\omega}}^{\frac{\alpha+\mu}{\omega}} \sin(\omega t)\mathrm{d}t = L_c\left(I_d\frac{\alpha}{\omega} + I_d\frac{\alpha+\mu}{\omega}\right) \tag{2}$$

where α is the firing angle; μ is the overlap angle; $I_d\frac{\alpha}{\omega}$ is the value of I_d at time $\frac{\alpha}{\omega}$; and $I_d\frac{\alpha+\mu}{\omega}$ is the value of I_d at time $\frac{\alpha+\mu}{\omega}$.

The right side of (2) is defined as the required commutation area S_N of the inverter during the commutation process:

$$S_N=L_c\left(I_d\frac{\alpha}{\omega}+I_d\frac{\alpha+\mu}{\omega}\right) \tag{3}$$

The left side of (2) is defined as the actual commutation area S_G that the AC side voltage can provide during the commutation process:

$$S_G=\sqrt{2}\,E\int_{\frac{\alpha}{\omega}}^{\frac{\alpha+\mu}{\omega}}\sin(\omega t)\mathrm{d}t \tag{4}$$

Therefore, the essence of the commutation process is the exchange of current between the commutation bridge arms through the equivalent commutation inductance, driven by the commutation voltage. The commutation process can be described by S_G and S_N. When $S_G=S_N$ is satisfied under the condition of $\pi-\alpha-\mu\ge\gamma_{\min}$ ($\gamma_{\min}$ is the minimum extinction angle), the commutation process can be successfully completed. Otherwise, CF will occur.

The process of H-LCC turning off current during AC faults can be divided into direct shutdown and transfer shutdown, depending on different topologies, as shown in Fig. 2. The direct shutdown directly turns off current when required. The transfer shutdown firstly transfers the current from the original branch to another branch, subsequently turning it off. Affected by the degree of AC faults, the current that the H-LCC needs to turn off has the following two situations, as shown in Fig. 3.

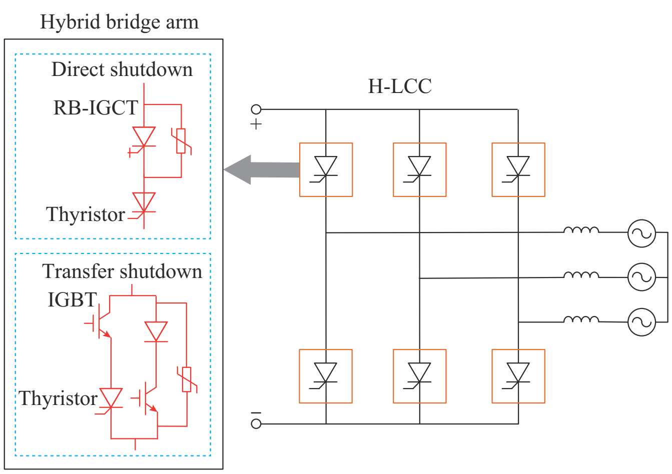

Fig. 2. Two typical topologies of H-LCC

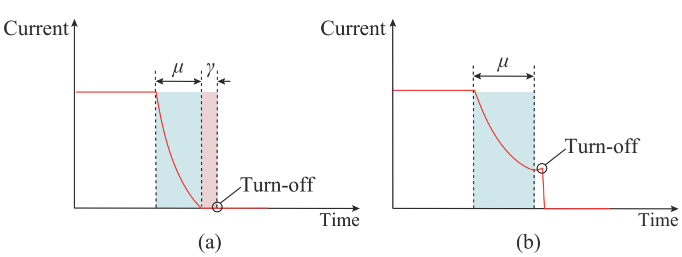

Fig. 3. Circuit shutdown mode of H-LCC. (a) $0<\gamma<\gamma_{\min}$. (b) $\gamma<0$.

When $0<\gamma<\gamma_{\min}$, the current in the bridge arm has a zero-crossing moment. However, the thyristor is unable to withstand the reverse voltage for the insufficient time, thus the blocking ability is not restored. When the forward voltage comes, the thyristor turns on again. In response to this situation, the gate drive unit of the fully controllable device detects the zero-crossing moment when the current in the bridge arm crosses zero, thereby initiating a self-shutdown signal to restore the blocking capability of the bridge arm. This situation can be regarded as an auxiliary shutdown mode, as shown in Fig. 3(a). When $\gamma<0$, the bridge arm is always in the commutation stage with current flowing. When the forward voltage arrives, the current moves back to the bridge arm again, causing the current to turn and rise. If the gate drive unit of the fully controllable device detects an abnormal change in $\mathrm{d}i/\mathrm{d}t$, an active shutdown signal is transmitted to force the current to zero, thereby completing the commutation. This mode can be regarded as forced shutdown mode, as shown in Fig. 3(b).

H-LCC needs to be governed by the natural commutation process of thyristor first, and reduces the turn-off current as much as possible. Then, fully controllable device is used to complete the commutation process at the last moment. The overall principle of the commutation process is not fundamentally different from LCC, which will not be distinguished in this paper.

B. Relationship Between Firing Angle and Reactive Power

The H-LCC adopts the same firing principle as LCC. Since the thyristor must be triggered to conduct after the corresponding natural commutation point, there is inevitable a lagging power factor on the AC side of the H-LCC. The correlation reference direction is adopted to analyze reactive power exchange. The 12-pulse inverter side is taken as an example, as shown in Fig. 4(a). The equivalent circuit on the inverter side of HVDC is shown in Fig. 4(b).

In the case of symmetrical operation and ignoring the reactive power generated by harmonic components, the total reactive power Q_i consumed by the 12-pulse inverter can be expressed as:

$$Q_i=P_d\tan\varphi=U_dI_d\tan\varphi \tag{5}$$

where P_d is the DC power; φ is the fundamental power factor angle; and U_d is the DC voltage. U_d of the two bridges in series can be expressed as:

$$U_d=2(U_{d0}\cos\gamma-R_cI_d)=U_{d0}(\cos\gamma-\cos\alpha) \tag{6}$$

where $R_c=3\omega L_c/\pi$ is the equivalent commutation impedance; and $U_{d0}=3\sqrt{6}\,E/(k\pi)$ is the ideal no-load DC voltage, and k is the converter transformer ratio. The reactive power compensation part of the AC filter and capacitor bank can be concentrated and equivalent to a three-phase capacitor bank with capacitive reactance X_f per phase. The reactive power can be expressed as:

$$Q_f=\frac{3E^2}{X_f} \tag{7}$$

The reactive power balance at the AC bus is considered as:

$$Q_s=-Q_i-Q_f \tag{8}$$

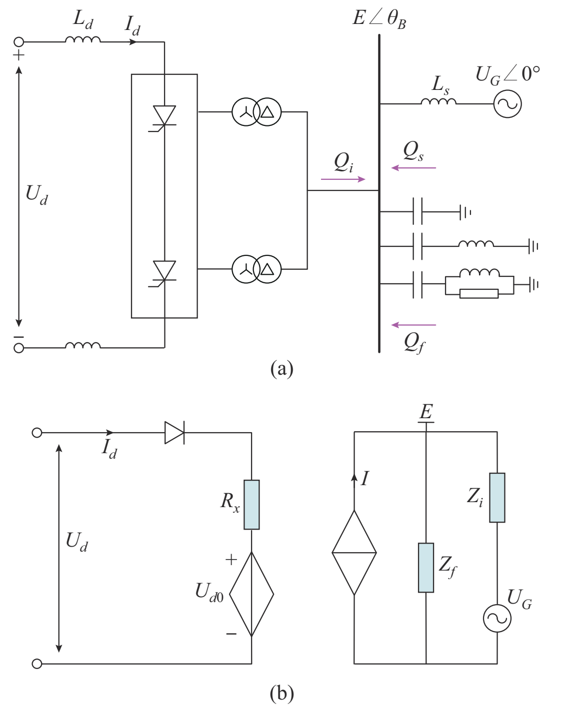

Fig. 4. Exchange of reactive power and equivalent circuit on inverter side. (a) 12-pulse inverter side. (b) Equivalent circuit on inverter side of HVDC.

where Q_s is the reactive power delivered by the AC system to the inverter-side commutation bus.

Due to $\mu=\pi-\alpha-\gamma$ and $\varphi=\frac{1}{2}[\cos\gamma+\cos(\gamma+\mu)]$, the reactive power delivered by the AC system to the inverter-side commutation bus can be obtained as:

$$Q_s=-(\cos\gamma-\cos\alpha)\tan\left(\frac{\pi}{2}+\frac{\alpha-\gamma}{2}\right)U_{d0}I_d-\frac{3E^2}{X_f} \tag{9}$$

α in (9) is derived as:

$$\frac{\partial Q_s}{\partial\alpha}=-\frac{\cos\gamma-\cos\alpha}{2}\left(1+\tan^2\left(\frac{\pi}{2}+\frac{\alpha-\gamma}{2}\right)\right)U_{d0}I_{d0}<0 \tag{10}$$

When the AC-side system fails, the system needs to provide more reactive power to the inverter. Taking the phase of the AC voltage as reference, the direction of power transfer to the bus is set to be positive. The relationship between the start-end voltage of the line and transmission power enables us to obtain:

$$E=\sqrt{(U_G+\Delta U)^2+(\delta U)^2}=\sqrt{\left(U_G-\frac{\omega L_s Q_s}{3U_G}\right)^2+\left(-\frac{\omega L_s P_d}{3U_G}\right)^2} \tag{11}$$

where U_G is the effective value of the phase voltage of the AC system; ΔU is the vertical component of the voltage; δU is the transverse component of the voltage; and L_s is the equivalent inductance of the AC bus.

C. Action Path After Firing Angle Changes

This paper further analyzes the impact of alterations in firing angle on the commutation process. The result of the commutation process can be characterized by γ. By changing (2), we can further obtain:

$$I_d(\alpha)+I_d(\alpha+\mu)=V\frac{\cos\gamma+\cos\alpha}{k} \tag{12}$$

where V is the inverter-side phase voltage amplitude. Assume β is the leading firing angle, $\beta=\pi-\alpha$. And when $\beta<60°$, $\beta=\gamma+\mu$.

From (12), we can know that the partial derivative $\partial\gamma/\partial\beta>0$. The decrease of α is used as an example. Reducing α can increase γ, which has a positive benefit on the commutation process. This direct action path is shown as path ① in Fig. 5.

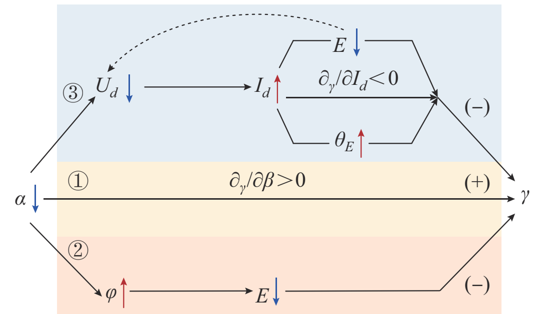

Fig. 5. Influence path of α on γ.

Concurrently, there are two other indirect action paths influenced by the interaction between the AC and DC systems. According to the analysis in Section II-B, the decrease of α increases φ and leads to the increase of reactive power absorbed by the inverter. This reduces the AC bus voltage and S_G, as shown in path ② in Fig. 5. It cannot be ignored that the decrease of α also reduces the DC voltage on the inverter side. This consequently leads to an increase in DC current and further affect γ. The influence can be divided into three aspects.

1) The increase in DC current directly increases S_N.

2) According to Fig. 4(b), E can also be expressed as:

$$\dot{E}=\underbrace{\frac{Z_fZ_i}{Z_f+Z_i}}_{Z_{IE}}\dot{I}+\underbrace{\frac{Z_f}{Z_f+Z_i}}_{Z_{EU}}\dot{U}_G \tag{13}$$

where Z_f is the filter impedance; Z_i is the Thevenin equivalent impedance of the AC system; $\dot{I}$ is the AC current phasor; $\dot{U}_G$ is the voltage phasor of AC system; $\dot{E}$ is the bus voltage phasor; Z_{IE} is the transfer coefficient from $\dot{I}$ to $\dot{E}$; and Z_{EU} is the transfer coefficient from $\dot{U}_G$ to $\dot{E}$.

Separate the real part and imaginary part of (13), we can obtain:

$$\begin{cases} E\cos\theta_B=\left|Z_{IE}\right|I\cos(\theta_B+\varphi+\theta_{ZIE})+\left|Z_{EU}\right|U_G\cos\theta_{ZEU} \\ E\sin\theta_B=\left|Z_{IE}\right|I\sin(\theta_B+\varphi+\theta_{ZIE})+\left|Z_{EU}\right|U_G\sin\theta_{ZEU} \end{cases} \tag{14}$$

where θ_B is the phase of $\dot{E}$; and θ_{ZIE} and θ_{ZEU} are the phase angles of Z_{IE} and Z_{EU}, respectively.

The relationship between I_d and inverter output current I is:

$$I=\frac{4\sqrt{3}}{\pi k}I_d \tag{15}$$

According to (14) and (15), I will also increase as the inverter-side I_d increases. The increase in the AC current amplitude will reduce E and increase the AC voltage phase θ_E, thereby reducing S_G. In addition, the reduction of E will further reduce U_d, creating a positive feedback loop $U_d \rightarrow I_d \rightarrow E \rightarrow U_d$.

3) Due to the tracking error of the phase locked loop (PLL), the increase in θ_E will make the actual firing angle larger. This effect of the indirect path ③ of the DC current has an important influence on the effectiveness of the firing control.

Therefore, the decrease of α has three main action paths on γ, namely one positive benefit path that increases γ and two negative benefit paths that decrease γ. The increase of α is just the opposite. The final impact result is determined comprehensively by the three action paths. In this paper, the result of γ increase caused by α change is called commutation positive benefit $Be+$, otherwise, it is called commutation negative benefit $Be-$.

III. Selected Analysis of H-LCC Firing Angle

The firing angle has an important influence on the commutation process, this paper chooses to optimize the firing angle provided by the original control system. According to the analysis in Section II-C, it should be ensured that $Be+$ is greater than $Be-$ after the adjustment of firing angle. This paper defines three boundaries and four states for the possible situations after changes in firing angle. The positions of these boundaries and the distance between each other are dynamically changed. They are not only related to the short-circuit ratio of the AC system and the current dynamics of the DC system, but also closely related to various factors such as the fault degree. Among them, state II and state III represent $Be+$ is greater than $Be-$. State I and state IV represent $Be-$ is greater than $Be+$. The left side of boundary 2 represents the direction in which the firing angle provided by the original control system is decreased, and the right side represents the direction for increasing the original firing angle, as shown in Fig. 6(a).

When AC fault is relatively slight, the reduction in commutation voltage and the increase in DC current are not significant at this time. If proper advanced firing is carried out on the basis of the original control, there is a situation that $Be+$ increased by the direct path is greater than $Be-$ brought by the indirect path, which belongs to state II. If the firing is too early and enter state I across boundary 1, the result will be the opposite. In this case, the grounded inductance value of the AC side is set to be in the range of $[H_x, H_y]$, as shown in Fig. 6(b). As the fault severity increases, the range of state II continues to decrease until it disappears and loses effect to suppress CF. At this time, after lagging firing is executed on the basis of the original control, $Be+$ brought by the indirect path begins to surpass $Be-$ brought by the direct path, and state III appears. It is obvious that when the firing comes too late, the start time of the commutation process will be too close to the arrival time of the forward voltage. Therefore, even if the lagging firing brings an increase in the commutation voltage, S_G will still be greatly reduced due to the short action time, and there must also be a boundary 3. Once crossing the boundary 3 and entering state IV, $Be-$ brought by the lagging firing will be greater than $Be+$ again, which renders the lagging firing ineffective.

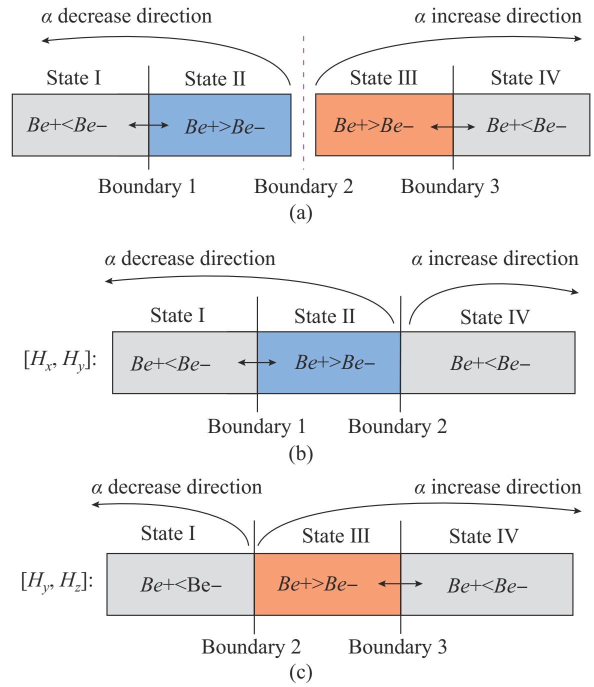

Fig. 6. Different states after firing angle is changed. (a) Two situations for firing angle optimization. (b) Advanced firing appropriate situation. (c) Lagging firing appropriate situation.

In this case, the AC-side grounded inductance value is set to be in the range of $[H_y, H_z]$, as shown in Fig. 6(c). When the AC-side grounded inductance value is in the range of $[H_x, H_y]$, advanced firing is effective, which is the principle of CFPREV. When the fault degree is a certain value H_a in the range of $[H_x, H_y]$, although the advanced firing is still in state II, the positive benefit obtained is not enough to meet the requirement of $\gamma_{\min}$. This will cause CF of LCC. However, H-LCC has the ability to self-shutdown the current, and it is not necessary to meet $\gamma_{\min}$ to ensure the smooth completion of commutation. Even when the fault level enters a more severe range of $[H_y, H_z]$, the situation in state III can still be exploited to defend against CF by lagging firing.

In actual LCC-HVDC projects, the control system adopts a combination of constant extinction angle, constant voltage, and constant current controls on the inverter side. If H-LCC adopts constant extinction angle control in primary controller, when AC fault occurs, the controller will maintain the mode of constant extinction angle. This will cause the firing angle to decrease continuously. When the fault degree is in the range of $[H_y, H_z]$, if the firing angle is not optimized accordingly, the control system may operate the H-LCC in state I. This will be detrimental to the bus voltage and make the H-LCC less effective in suppressing CF, which means that even if H-LCC has self-shutdown capability, the power transmission of the DC system will be affected. The deterioration of the commutation process will also impose higher requirement on the shutdown performance of H-LCC. At the moment of shutdown, if the maximum overvoltage that the fully controllable devices can withstand under the mixing ratio is exceeded, CF cannot be suppressed.

When the fault level only requires the H-LCC to execute auxiliary shutdown, the significance of optimizing the firing angle is minimal. The objective of this paper is to optimize the firing time in the forced shutdown mode. Lagging firing has become a major firing mode suitable for H-LCC. When $S_G=S_N$ cannot be satisfied under the condition of $(\pi-\alpha-\mu)\geq\gamma_{\min}$, the possible situations of S_G and S_N during the commutation process are presented, as shown in Fig. 7, where J is the moment when $\gamma=0$. Figure 7(a) is for a normal situation, and Fig. 7(b) and Fig. 7(c) are for two situations that exist in AC fault. Figure 7(b) represents that commutation process can ultimately be completed, but thyristor cannot restore blocking ability. Figure 7(c) represents that commutation process is still incomplete when the forward voltage is reached. In both situations, there is a value difference between S_N and S_G at $\gamma_{\min}$. When this difference is smaller, it indicates that the thyristor is closer to completing natural commutation by itself, and the commutation process is less affected by AC faults.

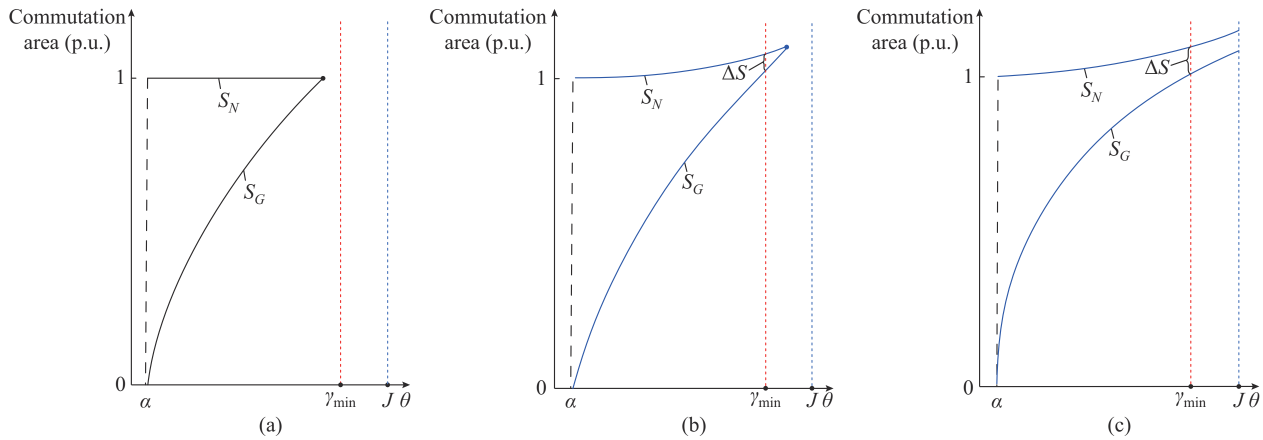

Fig .7. Changes in commutation area after firing. (a) Normal commutation area. (b) Auxiliary commutation area. (c) Forced commutation area.

The time point corresponding to $\gamma_{\min}$ can be selected as the reference line. The area difference $\Delta S=S_N-S_G$ at this moment is used to represent the relationship between Be+ and Be− after firing. When the change of the firing angle causes ΔS to continue to decrease, it means that Be+ of commutation is greater than Be−. Therefore, this paper defines the minimum value $\Delta S_{\min}$ of ΔS as the optimal commutation area difference. Then, the firing angle can exert the best ability of the inverter.

IV. FVF Method

A. Commutation Area Difference Prediction for Next Commutation Process

In order to obtain the impact of the change of firing angle on the next commutation process of H-LCC, it is necessary to obtain the prediction values of commutation voltage and DC current in advance to calculate the corresponding S_N and S_G. Equation (11) reflects the relationship between reactive power and commutation voltage, but it cannot be directly used to calculate the relationship between the two after a certain time interval. Therefore, this paper proposes a convenient prediction method based on correction coefficients.

The specific values of relevant parameters are obtained according to the last completed commutation, which are then substituted into (16).

$$Q_e=-P_{dl}\tan\left(\frac{\pi}{2}+\frac{\alpha_l-\gamma}{2}\right)-\frac{3{E_l}^2}{X_f} \tag{16}$$

where P_{dl} is the DC power of the last completed commutation at the time of firing; α_l is the firing angle of the last completed commutation; E_l is the commutation voltage when fired; and Q_e is the reactive power value obtained.

Q_e and the commutation voltage value E_f after commutation are substituted into (11). Then, $\omega L_s/3$ term in the equation is regarded as the unknown quantity M and M can be obtained by inverse calculation. M is brought into (17) to obtain the commutation voltage correction coefficient C_1.

$$C_1=M\frac{3}{\omega L_s} \tag{17}$$

In addition, every time a commutation process is completed, C_1 is updated again. For the next commutation process, we set α_{pre} as the firing angle, and substitute the relevant parameter values at this firing angle moment into (18).

$$Q_{e(pre)}=-P_{dn}\tan\left(\frac{\pi}{2}+\frac{\alpha_{pre}-\gamma}{2}\right)-\frac{3E_n^2}{X_f} \tag{18}$$

where E_n, P_{dn}, and $Q_{e(pre)}$ are the commutation voltage, DC power, and reactive power corresponding to α_{pre}, respectively. $Q_{e(pre)}$ and C_1 obtained from the last completed commutation process are substituted into (19), so as to obtain the predicted equivalent commutation voltage value E_{pre} after α_{pre} is fired.

$$E_{pre}=\sqrt{(U_G+\Delta U)^2+(\delta U)^2}=\sqrt{\left(U_G-C_1\frac{\omega L_s}{3}\frac{Q_{e(pre)}}{U_G}\right)^2+\left(-C_1\frac{\omega L_s}{3}\frac{P_d}{U_G}\right)^2} \tag{19}$$

The DC current prediction aims to obtain the average change rate of DC current after firing. When the DC current changes, the KVL equation of the inverter-side part of the DC system is:

$$U_c=L_d\frac{\mathrm{d}i_d}{\mathrm{d}t}+U_d+R_di_d \tag{20}$$

where U_c is the average voltage of the equivalent capacitance of the DC line to ground; U_d is the average DC voltage of the inverter-side port; and L_d and R_d are the equivalent inductance and resistance of the line, respectively.

The instantaneous change rate of DC current obtained by (20) cannot be directly used for prediction. Therefore, the same method for the commutation voltage prediction process is adopted. The average change rate k_a of the DC current is obtained based on the last completed commutation process. U_c and I_d corresponding to the firing moment and U_d after commutation are substituted into (20). Then, $1/L_d$ is replaced by the unknown quantity N, and N can be obtained by the inverse calculation. The DC current correction coefficient C_2 can be obtained as:

$$C_2 = NL_d \tag{21}$$

Every time a commutation process is completed, C_2 is updated again. For the upcoming commutation process, the relevant parameter values at the moment corresponding to α_{pre} and C_2 obtained from the last completed commutation process are substituted into (22). Then, the average change rate $k_{a(pre)}$ of the DC current can be predicted after firing.

$$k_{a(pre)} = \frac{C_2}{L_d}(U_c - U_d - R_d i_d) \tag{22}$$

The subsequent DC current can be obtained as:

$$I_{d(pre)} = I_d \frac{\alpha_{pre}}{\omega} + k_{a(pre)} \Delta t \tag{23}$$

where Δt is the time difference between α_{pre} and $\gamma_{\min}$.

When CF does not occur, C_1 and C_2 within a certain range can be used to correct the bias effect in prediction based on the quasi steady-state equations. Once CF occurs, the correction coefficients of adjacent commutation process will undergo significant changes, making them no longer applicable for predictive correction.

B. Implementation of FVF

Under normal circumstances, H-LCC still utilizes the firing angle given by the original control system. During the serious AC fault on the inverter side, it is necessary to optimize the firing angle by finding the optimal time to reduce the impact on the DC system. Therefore, FVF method is proposed to solve the problem, which is illustrated by taking the firing of the hybrid bridge arm VT_Y1 as an example, as shown in Fig. 8.

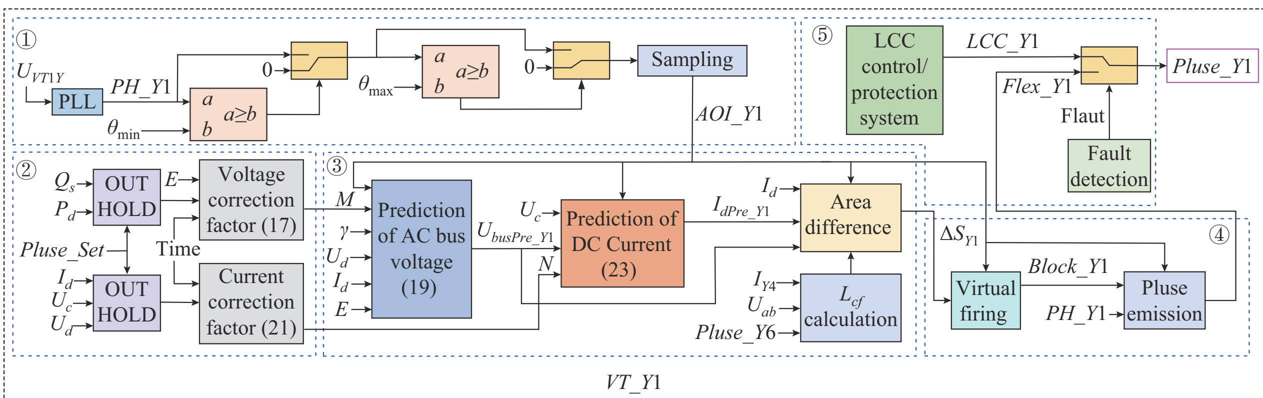

Fig. 8. Control chart for FVF.

The remaining 11 hybrid bridge arms also follow the similar process, and FVF is divided into 5 parts.

1) Part ①: after the commutation voltage U_{VT1Y} of the $Y1$ bridge arm enters the range that can be fired, PLL is used to obtain the synchronization phase value PH_Y1 of U_{VT1Y}. The specific selection range AOI_Y1 of the firing angle is delineated by $\theta_{\min}$ and $\theta_{\max}$, which are then passed to other corresponding modules, respectively. This section is updated according to the set sampling frequency. Meanwhile, every time AOI_Y1 is updated, the entire process in Fig. 8 will be re-executed.

2) Part ②: its function is data retention. In order to predict the relevant parameters in the next commutation process, it is necessary to calculate the correction coefficients from the data of the last completed commutation process. Relevant data are retained by controlling *Pluse_Set* signal to help calculate the correction coefficients. The data are updated until a new firing pulse is transmitted.

3) Part ③: its function is the prediction of ΔS_{Y1}, which is the commutation area difference associated with $Y1$ bridge arm. The firing angle corresponding to the synchronization phase is α_{pre}. It is assumed that bridge arms are triggered at α_{pre}, and the commutation voltage U_{busPre_Y1} and DC current I_{dPre_Y1} of the subsequent commutation process are predicted according to (19) and (23). In addition, due to the occurrence of AC faults, the equivalent commutation inductance will change. The new equivalent commutation inductance can be calculated from the commutation area based on the last completed commutation process. With the above steps, ΔS_{Y1} can be obtained in the upcoming commutation process.

4) Part ④: its function is to perform firing according to the real-time predicted value of ΔS_{Y1}, which is a dynamic search process. If ΔS_{Y1} does not meet the judging condition of $\Delta S_{\min}$ at this time, the pulse emission unit will be disabled through *Block_Y1* signal. This means that the firing behavior is virtually performed. Considering the remaining commutation time, this function waits for the AOI_Y1 to update again, and will not perform actual firing until it is determined that $\Delta S_{\min}$ is reached. The specific judgment condition is that if ΔS_{Y1} changes from decreasing to increasing, actual

firing can be performed near the turning point. Or when $\Delta S_{Y1}=0$, the actual firing can also be performed. The above process is further illustrated using Fig. 9 as an example. The time point corresponding to t_1-t_{n-1} belongs to virtual firing process without actual firing. If it is fired at time t_{n-1}, the change curves of S_N and S_G during the commutation process are represented by gray lines. The predicted result does not meet the judging condition of $\Delta S_{\min}$, and the firing pulse sending function is blocked as a virtual firing. Then, the module continues to calculate the next firing moment according to the sampling frequency. When firing at t_n, the change curves of S_N and S_G are represented by the blue line in the subsequent commutation process. If the predicted result at this firing angle meets the judging condition of $\Delta S_{\min}$, the blocking is released and the actual firing pulse *Flex_Y*1 is issued. Then, the commutation process begins.

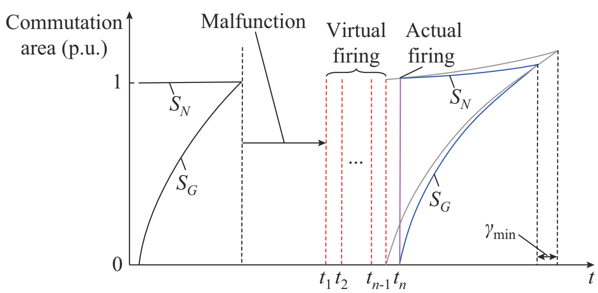

Fig. 9. Process of FVF.

5) Part ⑤: when the detection module detects that the AC fault occurs and firing angle needs to be optimized, *Flex_Y*1 given by the FVF will replace the firing pulse *LCC_Y*1 in the original control system. *Pluse_Y*1 is the final firing pulse received by the device in the bridge arm.

V. Example Verification and Analysis

The analysis performed above is not affected by H-LCCs of different topologies. Therefore, based on the CIGRE standard model in PSCAD/EMTDC software, this paper transforms the inverter side by taking the H-LCC topology of series RB-IGCT as an example. The proposed FVF method is added to the original control system for related verifications.

1) Case 1 represents the simulation results obtained using the original firing method, while Case 2 represents the simulation results obtained using the FVF method.

The single-phase grounded inductance value L_f of the AC bus on the inverter side is set to be 0.1 H. The fault duration is 0.1 s. The RB-IGCT mixing ratios adopted by H-LCC in Case 1 and Case 2 are both 65%. The change of firing angle during the fault period is shown in Fig. 10, which belongs to lagging firing. Figure 11(a) presents the DC current and Fig. 11(b) presents the DC voltage during AC fault. It can be observed that both schemes can successfully suppress the CF occurrence. However, the FVF method can effectively stabilize the fluctuations of DC voltage and current during fault period, maintaining DC power transmission, as shown in Fig. 11(c). Specifically, the shortage of DC power has decreased from 38.30% to 5.49%. Compared with Case 1, the reactive power absorbed by the H-LCC from the AC bus is reduced by 38.85%, as shown in Fig. 11(d). The longer the fault duration, the more obvious the difference between the two firing schemes. This effect helps maintain the bus voltage on the inverter side and recover the performance of the receiving-end system, as shown in Fig. 12. During the fault period, the total harmonic distortion (THD) of the three-phase bus voltage of the receiving-end system drops from 23.49%, 24.67%, 24.66% to 6.36%, 7.30%, 15.16%, respectively. At the same time, the peak overvoltage excess of the bus at the sending-end system is also reduced from 21.13% to 3.17%, as shown in Fig. 13, which is conducive to the security and stability of the sending-end system, especially when there is a high proportion of new energy access.

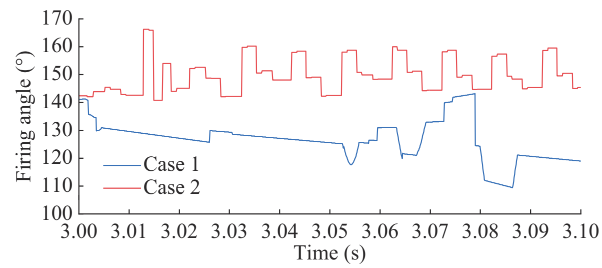

Fig. 10. Change of firing angle during fault period.

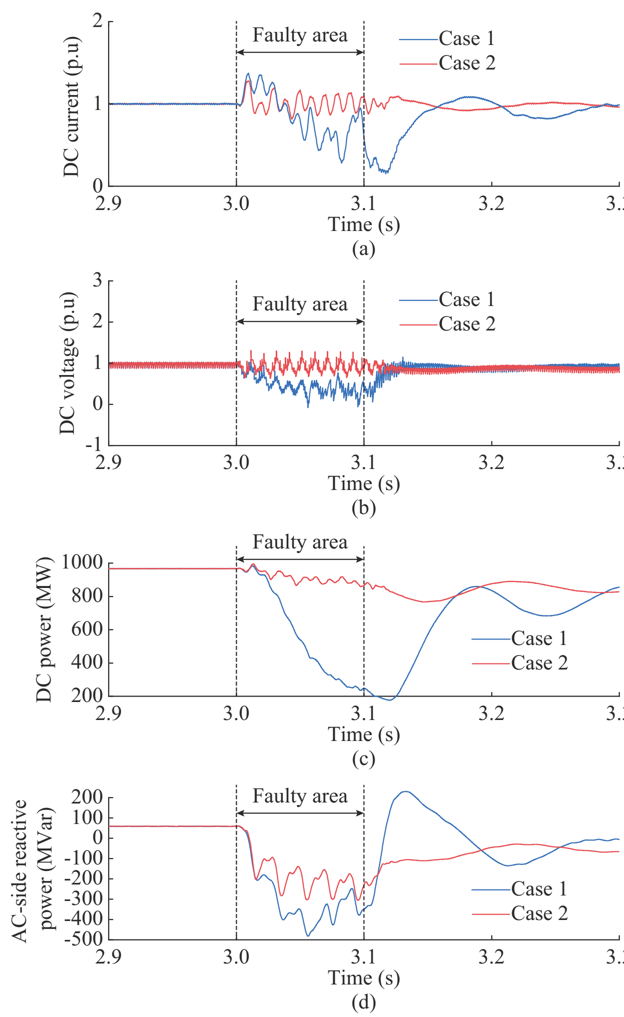

Fig. 11. Parameters change under single-phase fault. (a) DC current. (b) DC voltage. (c) DC power. (d) AC-side reactive power.

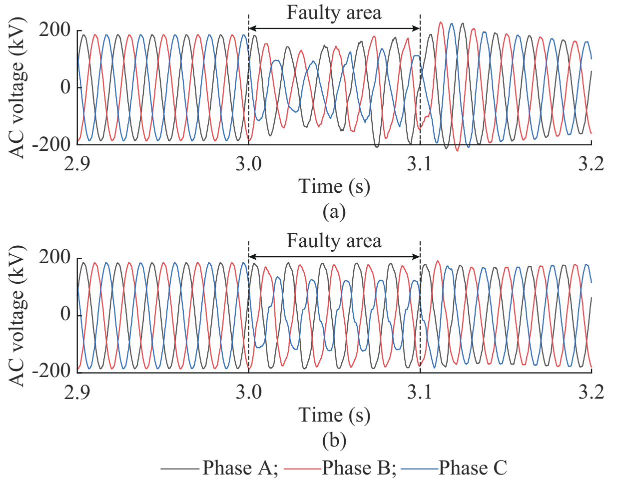

Fig. 12. Bus voltage of receiving-end system under single-phase fault. (a) Case 1. (b) Case 2.

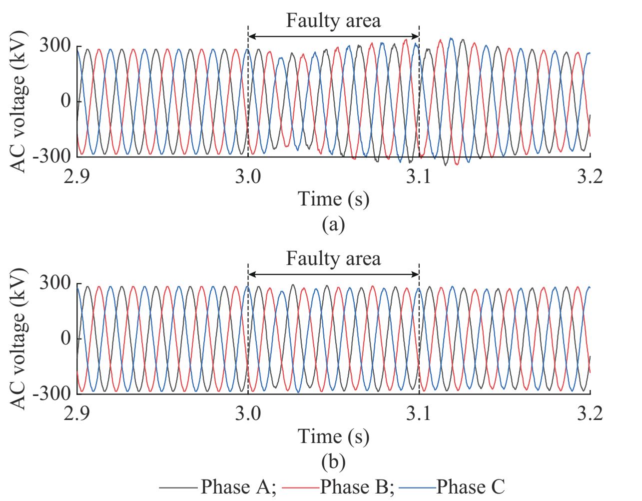

Fig. 13. Bus voltage of sending-end system under single-phase fault. (a) Case 1. (b) Case 2.

The three-phase grounded inductance value L_f of the AC bus on the inverter side is set to be 0.3 H. The fault duration is 0.1 s. The RB-IGCT mixing ratios adopted by H-LCC in Case 1 and Case 2 are both 65%. The change of firing angle under three-phase fault is shown in Fig. 14, which belongs to lagging firing.

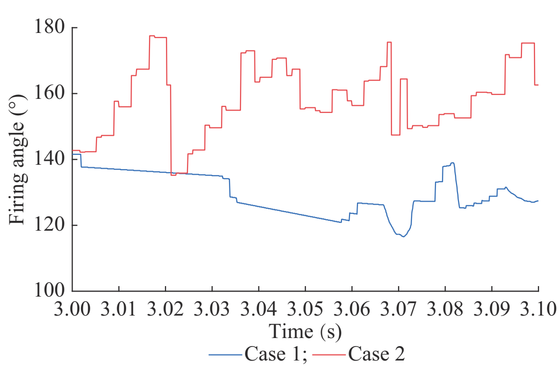

Fig. 14. Change of firing angle under three-phase fault.

Figure 15 shows that the FVF method can also achieve the expected results. The DC power transfer deficit during fault period is reduced from 32.31% to 3.36%, as shown in the Fig. 15(c). The absorption of reactive power has been reduced by 46.30% compared with that of Case 1, as shown in the Fig. 15(d). The THD of the three-phase voltage of the bus at the receiving end is reduced from 27.24%, 25.80%, 26.36% to 12.26%, 14.84%, 8.48%, respectively, as shown in the Fig. 16. The peak overvoltage excess is reduced from 19.37% to 5.98% in the sending-end system, as shown in the Fig. 17.

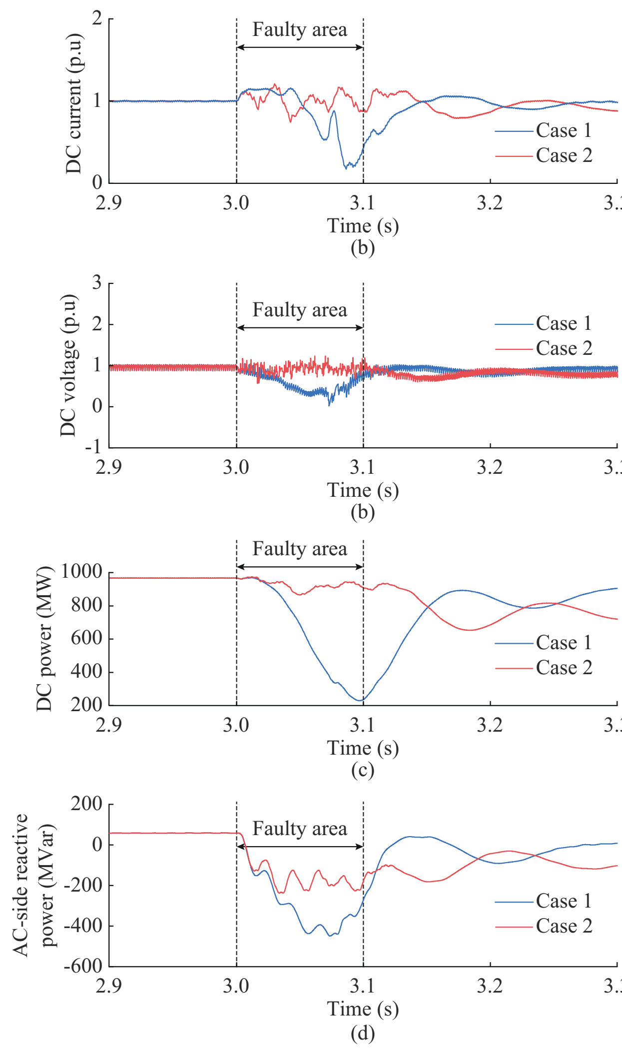

Fig. 15. Parameters change under three-phase fault. (a) DC current. (b) DC voltage. (c) DC power. (d) AC side-reactive power.

2) We then explore the critical fault inductance value that can cause CF and DC voltage drop to zero in different models. The smaller the critical fault inductance value, the stronger the ability of the model against CF. Case 1 represents the model with RB-IGCT mixing ratio of 30%. Case 2 represents the model with RB-IGCT mixing ratio of 30% using FVF method. Case 3 represents the model with RB-IGCT mixing ratio of 60%. Case 4 represents the model with RB-IGCT mixing ratio of 60% using FVF method. Phase-to-ground inductive faults are used at the inverter bus to investigate the performance of H-LCC and optimization method on CF mitigation.

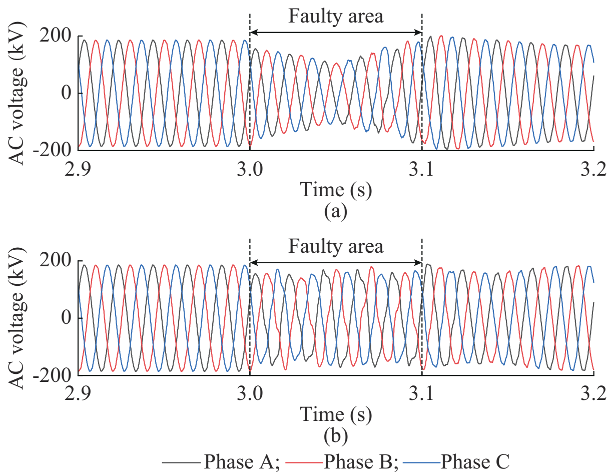

Fig. 16. Bus voltage of receiving-end system under three-phase fault. (a) Case 1. (b) Case 2.

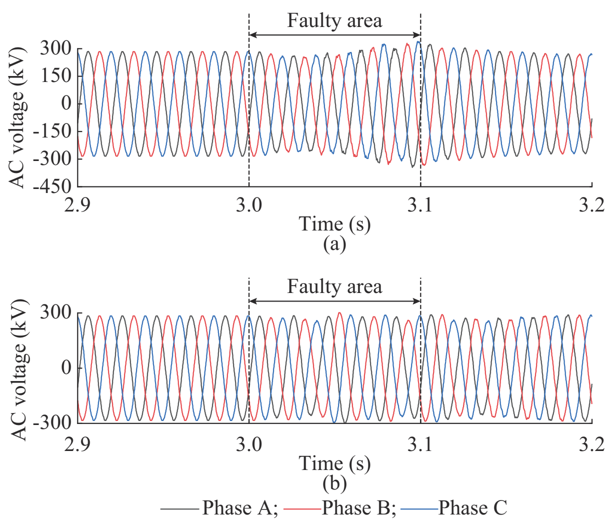

Fig. 17. Bus voltage of sending-end system under three-phase fault. (a) Case 1. (b) Case 2.

The fault duration is 0.1 s and is applied at different time in steps of 20°. The simulation result for single-phase fault condition is presented, as shown in Fig. 18. L_f of the CIGRE standard model is around 1.0 H [23]. Therefore, the H-LCC can significantly improve the defense ability of the converter against CF. The higher the mixing ratio, the stronger the defense ability. At the same time, it can be observed that the FVF method proposed in this paper can further enhance the defensive ability of H-LCC to withstand CF under the same mixing ratios.

VI. Conclusion

This paper takes the lack of a targeted firing angle method for H-LCC as the starting point of the research. By analyzing the influence mechanism of firing angle on the commutation process, the comprehensive action results of multiple paths are considered in the selection of firing angle. Combined with the characteristics of H-LCC, the concepts of dynamic boundary division and optimal commutation area difference are proposed.

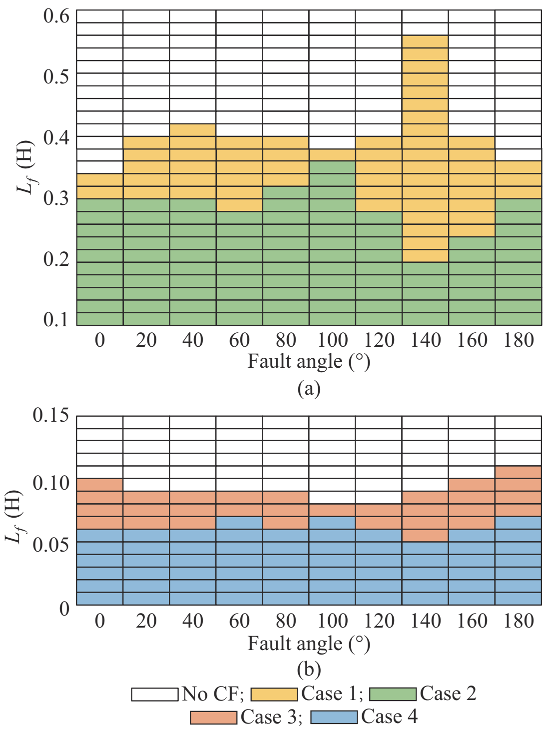

Fig. 18. Comparison of CF inhibition ability with different cases. (a) Cases 1 and 2. (b) Cases 3 and 4.

And the selection of firing angle is optimized by using the FVF method during the AC fault by means of prediction. The simulation results show that during the AC fault on the inverter side, the FVF method achieves smoother changes in DC current and voltage, which significantly improves the power transmission capability of the DC system and has a positive impact on the performance recovery of the receiving-end AC system and the stability of the sending-end AC system. At the same time, the FVF method can also improve the ability of the H-LCC to defense CF with the same mixing ratio, which is conducive to better exerting the advantages of H-LCC. In addition, the FVF method is only applicable to situations where CF has not occurred. In the future, we will study how to better handle the problems after CF in H-LCC.

References

[1] Y. Liu, X. Zhou, Q. Chen *et al.*, "Harmonic state space based impedance modeling and virtual impedance based stability enhancement control for LCC-HVDC systems," *Journal of Modern Power Systems and Clean Energy*, vol. 12, no. 1, pp. 287-298, Jan. 2024.

[2] Z. Wei, Y. Yuan, X. Lei *et al.*, "Direct-current predictive control strategy for inhibiting commutation failure in HVDC converter," *IEEE Transactions on Power Systems*, vol. 29, no. 5, pp. 2409-2417, Sept. 2014.

[3] L. Hong, X. Zhou, Y. Liu *et al.*, "Analysis and improvement of the multiple controller interaction in LCC-HVDC for mitigating repetitive commutation failure," *IEEE Transactions on Power Delivery*, vol. 36, no. 4, pp. 1982-1991, Aug. 2021.

[4] C. Zheng, Y. Tang, and Z. Li, "Coordinated control strategy for cascading commutation failure mitigation considering reactive power interaction," *IEEE Transactions on Power Delivery*, vol. 37, no. 4, pp. 3225-3234, Aug. 2022.

[5] W. Yao, C. Liu, J. Fang *et al.*, "Probabilistic analysis of commutation failure in LCC-HVDC system considering the CFPREV and the initial fault voltage angle," *IEEE Transactions on Power Delivery*, vol. 35,

no. 2, pp. 715-724, Apr. 2020.
[6] D. Tian and X. Xiong, "Corrections of original CFPREV control in LCC-HVDC links and analysis of its inherent plateau effect," *CSEE Journal of Power and Energy Systems*, vol. 8, no. 1, pp. 10-16, Jan. 2022.
[7] S. Mirsaeidi, X. Dong, D. Tzelepis *et al*., "A predictive control strategy for mitigation of commutation failure in LCC-based HVDC systems," *IEEE Transactions on Power Electronics*, vol. 34, no. 1, pp. 160-172, Jan. 2019.
[8] S. Gomes, N. Martins, T. Jonsson *et al*., "Modeling capacitor commutated converters in power system stability studies," *IEEE Transactions on Power Systems*, vol. 17, no. 2, pp. 371-377, May 2002.
[9] K. Sadek, M. Pereira, D. P. Brandt *et al*., "Capacitor commutated converter circuit configurations for DC transmission," *IEEE Transactions on Power Delivery*, vol. 13, no. 4, pp. 1257-1264, Oct. 1998.
[10] C. Guo, C. Li, C. Zhao *et al*., "An evolutional line-commutated converter integrated with thyristor-based full-bridge module to mitigate the commutation failure," *IEEE Transactions on Power Electronics*, vol. 32, no. 2, pp. 967-976, Feb. 2017.
[11] C. Guo, Z. Yang, B. Jiang *et al*., "An evolved capacitor-commutated converter embedded with antiparallel thyristors based dual-directional full-bridge module," *IEEE Transactions on Power Delivery*, vol. 33, no. 2, pp. 928-937, Apr. 2018.
[12] R. Zhan, C. Zhao, Z. Hai *et al*., "Scheme design and mechanism analysis of line commutated converter based on fully controlled resistance-capacitance module," *Power System Technology*, vol. 46, no. 2, pp. 532-540, Feb. 2022.
[13] H. Rao, Y. Zhou, S. Xu *et al*., "Key technologies of ultra-high voltage hybrid LCC-VSC MTDC systems," *CSEE Journal of Power and Energy Systems*, vol. 5, no. 3, pp. 365-373, Sept. 2019.
[14] W. Zhang, L. Chen, X. Wei *et al*., "Design and operation mode of based on controllable current source converter HVDC system," *Proceedings of the CSEE*, vol. 42, no. 7, pp. 2532-2541, Apr. 2022.
[15] R. Zhan, W. Ye, J. Xia *et al*., "Coupled turn-off model and coordination strategy of semi-controlled and full-controlled devices in series," *Proceedings of the CSEE*, vol. 43, no. 10, pp. 3949-3961, May 2023.
[16] C. Gao, J. Yang, Z. He *et al*., "Novel controllable-line-commutated converter for eliminating commutation failures of LCC-HVDC system," *IEEE Transactions on Power Delivery*, vol. 38, no. 1, pp. 255-267, Feb. 2023.
[17] R. Zeng, B. Zhao, T. Wei *et al*., "Integrated gate commutated thyristor-based modular multilevel converters: a promising solution for high-voltage dc applications," *IEEE Industrial Electronics Magazine*, vol. 13, no. 2, pp. 4-16, Jun. 2019.
[18] C. Xu, B. Zhao, X, Zhang *et al*., "Full-time junction temperature extraction of IGCT based on electro-thermal model and TSEP method for high-power applications," *IEEE Transactions on Industrial Electronics*, vol. 68, no. 1, pp. 47-58, Jan. 2021.
[19] C. Xu, Z. Yu, Z. Chen *et al.*, "Comprehensive analysis and experiments of RB-IGCT, IGCT with fast recovery diode and standard recovery diode in hybrid line-commutated converter for commutation failure mitigation," *IEEE Transactions on Industrial Electronics*, vol. 70, no. 2, pp. 1126-1139, Feb. 2023.
[20] C. Xu, Z. Yu, B. Zhao *et al.*, "A novel hybrid line commutated converter based on IGCT to mitigate commutation failure for high-power HVDC application," *IEEE Transactions on Power Electronics*, vol. 37, no. 5, pp. 4931-4936, May 2022.
[21] C. Xu, Z. Yu, B. Zhao *et al.*, "Hybrid line commutated converter with fast commutation characteristic based on IGCT for HVDC application: topology, design methodology, and experiments," *IEEE Transactions on Power Electronics*, vol. 38, no. 4, pp. 4668-4679, Apr. 2023.
[22] Z. Wang, C. Xu, Z. Yu *et al*., "Low-frequency and sub-synchronous power oscillation suppression and analysis of hybrid line commutated converter for HVDC grid," *IEEE Transactions on Power Systems*, vol. 39, no. 2, pp. 4127-4137, Feb. 2024.
[23] R. Zhu, X. Zhou, H. Xia *et al*., "DC current order optimization based strategy for recovery performance improvement of LCC-HVDC transmission systems," *Journal of Modern Power Systems and Clean Energy*, vol. 11, no. 3, pp. 1020-1026, May 2023.

Jianchao Ma received the B.S. degree in electrical engineering from Henan Polytechnic University, Jiaozuo, China, in 2018, and the M. S. degree in electrical engineering from Guangxi University, Nanning, China, in 2022. He is currently working toward the Ph. D. degree in electrical engineering with the College of Electrical and Information Engineering, Hunan University, Changsha, China. His research interests include high-voltage direct current system and power electronic device in power system.

Xiaoping Zhou received the B.S. and Ph.D. degrees in electrical engineering from Hunan University, Changsha, China, in 2013 and 2018, respectively. He is currently working as an Associate Professor of electrical engineering with Hunan University. His research interests include high-voltage direct current system, distributed generation, microgrid, power quality, and energy storage.

Lingfeng Deng received the B.S. degree in electrical engineering from China University of Mining and Technology, Xuzhou, China, in 2018, and the M. S. degree in electrical engineering from Hunan University, Changsha, China, in 2021. He is currently working toward the Ph.D. degree in Hunan University. His research interests include high-voltage direct current system and application of novel power electronic device in power system.

Lerong Hong received the B.S. and Ph.D. degrees in electrical engineering from Hunan University, Changsha, China, in 2016, and 2021, respectively. He is currently working as an Associate Professor of electrical engineering with Hunan University. His research interests include high-voltage direct current system and power electronic converter.

Hanting Peng received the B.S. degrees in electrical engineering from Hunan University, Changsha, China, in 2021. He is currently working toward the Ph.D. degree in Hunan University. His research interests include power electronic converter and high-voltage direct current system.

Yizhen Hu received the B.S. degrees in electrical engineering from Henan University of Technology, Zhengzhou, China, in 2020. He is currently working toward the Ph.D. degree in Hunan University, Changsha, China. His research interest includes power electronic converter.

Lei Zhang received the B.S. degree in electrical engineering from Guizhou University, Guiyang, China, in 2021. He is currently working toward the Ph.D. degree in Hunan University, Changsha, China. His research interests include power electronic converter and energy storage.

Fenfen Zhu received the B.S. degree in electrical engineering from Anhui University, Hefei, China, in 2021, and the M.S. degree in electrical engineering from Hunan University, Changsha, China, in 2024. In 2024, she joined State Grid Wuhu Electric Power Supply Company, Wuhu, China. Her research interest includes power electronic converter.

Haitao Xia received the B.S. and Ph.D. degrees in electrical engineering from Hunan University, Changsha, China, in 2017, and 2022, respectively. In 2022, he joined China Railway Construction Heavy Industry Corporation Limited, Changsha, China. His research interests include high-voltage direct current system and dynamic analysis of power electronic converter.

Honglin Ouyang received the B.S., M.S., and Ph.D. degrees from Hunan University, Changsha, China, in 1982, 1992, and 2005, respectively. Since 2002, he has been a Professor of electrical engineering with the Department of Electrical and Information Engineering, Hunan University. His research interests include electric power saving, reactive power compensation, and active power filter.